

Testing the CKM unitarity at high energy via the W^+W^- production at the LHC and future colliders

E. Gabrielli^{a,b,c}, L. Marzola^{c,d} and K. Mürsepp^c

(a) *Physics Department, University of Trieste, Strada Costiera 11, I-34151 Trieste, Italy*

(b) *INFN, Sezione di Trieste, Via Valerio 2, I-34127 Trieste, Italy*

(c) *Laboratory of High-Energy and Computational Physics, NICPB, Rävåla pst 10, 10143 Tallinn, Estonia*

(d) *Institute of Computer Science, University of Tartu, Narva mnt 18, 51009 Tartu, Estonia*

ABSTRACT

We propose a novel test to assess the unitarity of the Cabibbo-Kobayashi-Maskawa matrix, V_{CKM} , at present and future collider experiments. Our strategy makes use of the W^+W^- production cross section to directly probe the $V_{\text{CKM}}^\dagger V_{\text{CKM}}$ product, which regulates the high-energy behavior of the observable. The violation of unitarity is signalled by an anomalous behavior of the cross section that grows quadratically with the W^+W^- invariant mass with respect to the Standard Model prediction. By using the recent ATLAS measurements of the W^+W^- cross section we are able to constrain the maximal unitarity violation allowed by current data, producing a bound complementary to the results of flavor physics experiments. Forecasts for the high luminosity phase of the LHC and for the future 100 TeV hadron collider are also discussed.

1 Introduction

The Standard Model (SM) quark flavor mixing arises from a misalignment between the Yukawa coupling matrices of up- and down-type quarks. The effect is measurable in the charged-current (cc) interactions mediated by the W^\pm gauge bosons and is parameterized by the Cabibbo-Kobayashi-Maskawa [1, 2] (CKM) matrix, V_{CKM} , appearing in the related interaction Lagrangian

$$\mathcal{L}^{cc} = -\frac{g}{\sqrt{2}} (\bar{u}_L, \bar{c}_L, \bar{t}_L) \gamma^\mu W_\mu^+ V_{\text{CKM}} \begin{pmatrix} d_L \\ s_L \\ b_L \end{pmatrix} + h.c., \quad V_{\text{CKM}} = \begin{pmatrix} V_{ud} & V_{us} & V_{ub} \\ V_{cd} & V_{cs} & V_{cb} \\ V_{td} & V_{ts} & V_{tb} \end{pmatrix}, \quad (1.1)$$

where u, c, t and b, s, t stand for the corresponding up and down quark fields.

The CKM matrix is necessarily unitary within the SM: it is given by the product of the unitary matrices that connect gauge and mass eigenstates. The unitarity condition is expressed as

$$\sum_i V_{ij} V_{ik}^* = \delta_{jk} \quad \text{or} \quad \sum_j V_{ij} V_{kj}^* = \delta_{ik}, \quad (1.2)$$

where the indices i and j run on the up- or the down-type quark fields, respectively. Each of these conditions yields nine independent constraints, six of these can be represented as triangles in a complex plane.

Experimental tests of unitarity in quark mixing probe combinations of the above conditions and have the potential to unveil the presence of new physics should anomalies be detected [3]. For instance, models including new fields that mix with quarks in charged-current weak interactions typically entail a violation of unitarity at energies below the mass scale characteristic of the new degrees of freedom. Currently, independent measurements of the CKM matrix elements give for the 1st and 2nd row of the matrix [4],

$$|V_{ud}|^2 + |V_{us}|^2 + |V_{ub}|^2 = 0.9985 \pm 0.0007, \quad (1.3)$$

$$|V_{cd}|^2 + |V_{cs}|^2 + |V_{cb}|^2 = 1.001 \pm 0.012, \quad (1.4)$$

while for the 1st and 2nd column we have [4],

$$|V_{ud}|^2 + |V_{cd}|^2 + |V_{td}|^2 = 0.9972 \pm 0.0020 \quad (1.5)$$

$$|V_{us}|^2 + |V_{cs}|^2 + |V_{ts}|^2 = 1.004 \pm 0.012. \quad (1.6)$$

Another independent test for the second row of the matrix, obtained from the measurement of $\sum_{u,c,d,s,b} |V_{ij}|^2$ by subtracting the total contribution of the first row, gives [4]

$$|V_{cd}|^2 + |V_{cs}|^2 + |V_{cb}|^2 = 1.002 \pm 0.027. \quad (1.7)$$

In order to quantify possible deviations from unitarity in charged current interactions, we introduce the diagonal parameters δ_q , with $q = u, d, s, c, b$, defined as

$$\delta_q \equiv \begin{cases} |V_{qd}|^2 + |V_{qs}|^2 + |V_{qb}|^2 - 1 & \text{for } q = u, c \\ |V_{uq}|^2 + |V_{cq}|^2 + |V_{tq}|^2 - 1 & \text{for } q = d, s, b. \end{cases} \quad (1.8)$$

As we can see from the above results, the CKM unitarity tests are presently well in agreement with SM expectations, although a 2.2σ tension concerning δ_u is present. The discrepancy, dubbed ‘‘Cabibbo

angle anomaly”, [5–10] is mainly due to the recent determination of the $|V_{ud}|$ element from the super-allowed $0^+ \rightarrow 0^+$ nuclear β decays [5]. However, it is fair to say that the discrepancy depends on which $|V_{ud}|$ measurement is considered in global fit. For instance, Ref. [6] finds $\delta_u = -0.00151(53)$, corresponding to a 2.85σ deviation that could be further amplified by using only the most constraining measurements of V_{ud} in the global fit. We refer the reader to Refs. [6, 11–17] for new physics interpretations of the Cabibbo angle anomaly.

Currently, the CKM matrix unitarity tests encoded in the δ_q parameters rely on the cancellation between the unity and the sum of the involved squared matrix elements, which are generally individually measured. This methodology affects the power of the test as the outcome strongly depends on the precision level at which each matrix element is measured. It would then be desirable to have a further independent test of unitarity that could directly gauge the parameters δ_q , thereby bypassing the problems posed by the determination of the individual contributions. As we show in the following, measurements of the W^+W^- production cross section at hadron colliders provide the means to achieve exactly that.

The process $pp \rightarrow W^+W^-$ is known to be a powerful tool for constraining new physics models affecting SM precision observables [18–23]. In order to test unitarity in charged current interactions, we make use of the related tree-level amplitude and analyze the interplay between the divergent s -channel term, driven by the longitudinal modes of the produced gauge bosons, and the quark contributions weighted by the CKM matrix elements under the customary assumption that neutral currents are not modified. Whereas gauge invariance and the unitarity of the CKM matrix ensure an exact cancellation in the SM, the cancellation does not occur in the presence of non-vanishing δ_q parameters. As a result, the loss of unitarity yields an anomalous contribution to the cross section that grows quadratically with the partonic center of mass energy or, analogously, with the W^+W^- invariant mass. Importantly, the magnitude of the anomalous term is proportional to δ_q and measurements of the $pp \rightarrow W^+W^-$ cross section at colliders can then be used to directly constrain the parameter.

Recent measurements of this observable by the CMS [24–26] and ATLAS [27–30] collaborations are found to be in good agreement with SM predictions [31–34]. We utilize the data to assess the power of the LHC to constrain unitarity in the quark mixing and extend the analysis to gauge the reach of the planned high-luminosity phase, as well as of the future hadron collider running at 100 TeV [35, 36].

2 WW production via quark fusion

The W^+W^- states of interest are mainly produced at proton colliders via electroweak processes in a continuous range of diboson invariant masses, m_{WW} . The corresponding hadronic differential cross section can be written as

$$\frac{d\sigma}{d\Omega dm_{WW}} = \frac{\beta_W}{64\pi^2 m_{WW}^2} \sum_{q=u,d,s,c,b} |\overline{\mathcal{M}}^{q\bar{q}}|^2 L^{q\bar{q}}(\tau), \quad (2.1)$$

where $\beta_W = \sqrt{1 - 4M_W^2/m_{WW}^2}$, $\tau = m_{WW}/\sqrt{S}$, M_W is the W boson mass and \sqrt{S} is the center of mass energy of the pp system. The infinitesimal solid angle expressed in polar coordinates is $d\Omega = d\cos\Theta d\varphi$, with Θ being the scattering angle in the center of mass frame of reference (CM) for the partonic process $q\bar{q} \rightarrow W^+W^-$ and φ the azimuthal angle. The unpolarized squared amplitude $|\overline{\mathcal{M}}^{q\bar{q}}|^2$ of the partonic process, mediated over initial states, is weighted by the parton luminosity $L^{q\bar{q}}(\tau)$ of the specific $q\bar{q}$ initial state

$$L^{q\bar{q}}(\tau) = \frac{4\tau}{\sqrt{S}} \int_{\tau}^{1/\tau} \frac{dz}{z} q_q(\tau z) q_{\bar{q}}\left(\frac{\tau}{z}\right), \quad (2.2)$$

where $q_q(x)$ and $q_{\bar{q}}(x)$ are the parton distribution function (PDF) of the parton q and antiparton \bar{q} , respectively. We use the recent (PDF4LHC21) release [37], for $\sqrt{S} = 13$ TeV and factorization scale m_{WW} , when deriving the unitarity bounds with current LHC data.

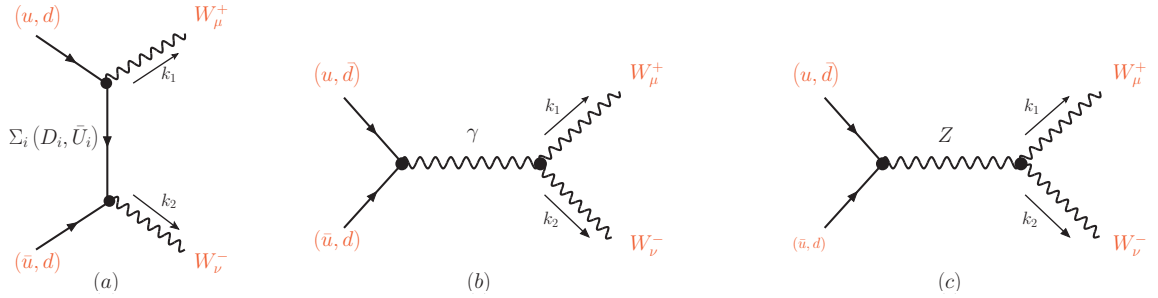


Figure 1: Feynman diagrams for the processes $pp \rightarrow W^+W^-$ initiated by first generation quarks. The symbols $U_i = \{u, c, t\}$ and $D_i = \{d, s, b\}$ indicate up and down-type quarks, respectively. We neglect diagrams mediated by the Higgs boson considering the limit of massless quarks in the initial state. The arrows on the fermion lines indicate the momentum flow. We indicate with k_1 and k_2 the (outgoing) W^+ and W^- 4-momenta.

The tree-level Feynman diagrams contributing to the underlying partonic process $\bar{q}(p_1)q(p_2) \rightarrow W^+(k_1)W^-(k_2)$ are shown in Fig. 1 for the case of first generation quarks. For the purpose of the present analysis we can work in the high energy approximation in which all quark masses can be neglected—including the top-quark mass, as discussed at the end of this section. The amplitude for the process is then written as

$$\mathcal{M}^{q\bar{q}} = -ie^2 \left[\bar{v}(p_1) \Gamma_{\mu\nu}^q u(p_2) \right] \varepsilon^\mu(k_1)^* \varepsilon^\nu(k_2)^*, \quad (2.3)$$

where we indicated with $\varepsilon^\mu(k_1)$ and $\varepsilon^\nu(k_2)$ the polarization vectors of W^+ and W^- , respectively. The effective vertex $\Gamma_{\alpha\beta}^q$ is given under the massless quark approximation by

$$\begin{aligned} \Gamma_{\mu\nu}^{q=u,c} &= \frac{1}{s} (\gamma^\alpha \bar{g}_V^q - \gamma^\alpha \gamma_5 \bar{g}_A^q) V_{\alpha\nu\mu}(p, -k_2, -k_1) + \frac{\xi_q}{4ts_W^2} \gamma_\nu (\not{p}_2 - \not{k}_1) \gamma_\mu (1 - \gamma_5), \\ \Gamma_{\mu\nu}^{q=d,s,b} &= \frac{1}{s} (\gamma^\alpha \bar{g}_V^q - \gamma^\alpha \gamma_5 \bar{g}_A^q) V_{\alpha\nu\mu}(p, -k_2, -k_1) + \frac{\xi_q}{4us_W^2} \gamma_\nu (\not{p}_2 - \not{k}_2) \gamma_\mu (1 - \gamma_5), \end{aligned} \quad (2.4)$$

with $s_W = \sin \theta_W$ and θ_W the Weinberg angle, e being the unit electric charge and $p = k_1 + k_2$. The parameter $\xi_q \equiv \sum_{D=d,s,b} [V_{qD}^* V_{qD}]$ for $q = u, c$ and $\xi_q \equiv \sum_{U=u,c,t} [V_{Uq}^* V_{Uq}]$ for $q = d, s, b$, model the CKM unitarity condition— $\xi_q = 1$ in the SM—and arise from the diagram (a) in Fig. 1. The effective couplings $\bar{g}_{V,A}^q$ in Eq. (2.4) are given by

$$\bar{g}_V^q = Q^q + \frac{g_V^q \chi}{s_W^2}, \quad \bar{g}_A^q = \frac{g_A^q \chi}{s_W^2}, \quad \chi = \frac{s}{2(s - M_Z^2)}, \quad (2.5)$$

where M_Z is the Z boson mass, $g_V^q = T_3^q - 2Q^q s_W^2$, $g_A^q = T_3^q$ and T_3^q and Q^q are the isospin and electric charge (in unit of e) of the quark q . The χ term in Eq. (2.5), which weights the contribution of the virtual Z channel, is real since we neglect the Z width contribution. The function $V_{\alpha\nu\mu}(k_1, k_2, k_3)$ is the Feynman rule of the trilinear vertex $V_\alpha(k_1) W_\nu^+(k_2) W_\mu^-(k_3)$, $V \in \{\gamma, Z\}$, given by

$$V_{\alpha\nu\mu}(k_1, k_2, k_3) = (k_1 - k_2)_\mu g_{\alpha\nu} + (k_2 - k_3)_\alpha g_{\mu\nu} + (k_3 - k_1)_\nu g_{\alpha\mu}, \quad (2.6)$$

for incoming momenta in the trilinear vertex: ($k_1 + k_2 + k_3 = 0$). The Mandelstam variables s, t and u appearing in the above equations are given by

$$s = (p_1 + p_2)^2, \quad t = (p_2 - k_1)^2, \quad u = (p_2 - k_2)^2, \quad (2.7)$$

where s coincides with the diboson invariant mass $s = m_{WW}^2$.

In order to investigate the effects of unitarity violation we introduce the parametrization

$$\xi_q = 1 + \delta_q \quad (2.8)$$

in the effective vertex $\Gamma_{\mu\nu}^q$ defined in Eq. (2.4) and for δ_q given in Eq. (1.8). Then, the unpolarized square amplitude for the process $q\bar{q} \rightarrow W^+W^-$, mediated over initial spin and color degrees of freedom, is given by

$$|\overline{\mathcal{M}}^{q\bar{q}}|^2(\delta_q) = |\overline{\mathcal{M}}_{\text{SM}}^{q\bar{q}}|^2 + \delta_q \Delta\overline{\mathcal{M}}_1^{q\bar{q}} + \delta_q^2 \Delta\overline{\mathcal{M}}_2^{q\bar{q}}, \quad (2.9)$$

where $|\overline{\mathcal{M}}_{\text{SM}}^{q\bar{q}}|^2$ is the SM contribution¹ and the extra terms vanish in absence of unitarity violation. By retaining only the leading orders in the $s/M_W^2 \gg 1$ expansion, we find

$$\begin{aligned} \Delta\overline{\mathcal{M}}_1^{q\bar{q}} &\simeq \frac{\alpha^2 \pi^2}{6N_c s_W^4} \left(\frac{s}{M_W^2} \right) s_\Theta^2 \left[6 - \frac{M_Z^2}{M_W^2} (3 - 4x_q s_W^2) \right], \\ \Delta\overline{\mathcal{M}}_2^{q\bar{q}} &\simeq \frac{\alpha^2 \pi^2}{4N_c s_W^4} \left[\left(\frac{s^2}{M_W^4} \right) s_\Theta^2 + \left(\frac{s}{M_W^2} \right) 4(3 + c_\Theta^2) \right]. \end{aligned} \quad (2.10)$$

In the equation above, $x_q = 1, 1/2$ for up- (U) and down-type (D) quarks respectively and $N_c = 3$ is the number of colors. We also defined $c_\Theta = \cos \Theta$ and $s_\Theta = \sin \Theta$, with Θ being the scattering angle formed by the quark and W^- momenta in the CM frame. In our numerical analysis we use the exact analytical results for the above anomalous contributions, given in the appendix A as functions of s and Θ .

Concerning the parametrization in Eq. (2.8), we perform our analysis considering constant values for the parameters δ_q , that is independent of the partonic CM energy \sqrt{s} . This scaling is expected to hold at energies below the characteristic scale Λ where the new physics effects restore unitarity. We assume Λ to be much larger than the energies explored at the considered collider experiments and do not speculate on the origin of this effective scale to retain independence from the specifics of the UV complete theory.

As anticipated, we neglect the top-quark mass (m_t) corrections that appear in processes initiated by down-type quarks through a virtual top exchange. For $d\bar{d}$ and $s\bar{s}$ initial states, these contributions are proportional to $\mathcal{O}(m_t^2/m_{WW}^2|V_{td}|^2)$ and $\mathcal{O}(m_t^2/m_{WW}^2|V_{ts}|^2)$, respectively, in both the SM and the anomalous contributions. Since the relevant m_{WW} region for constraining the $\delta_{d,s}$ parameters lies in the range of invariant masses $m_{WW} \gtrsim 1$ TeV, taking into account the suppression of the off-diagonal terms in the CKM matrix elements yields corrections well below the per mille level. For $b\bar{b}$ quark initial states, instead, $V_{tb} \sim 1$ results in much larger top mass corrections of the order of a few percent in the relevant region $m_{WW} \gtrsim \text{TeV}$. However, since the bounds provided with our method on δ_b are at a 5-10% precision level, we can still safely neglect these top-quark mass effects.

3 Bounds on the unitarity violation parameters

The ATLAS [29, 30] and CMS [26, 38] collaborations have recently measured the $pp \rightarrow W^+W^-$ cross section at the LHC run2 using $\mathcal{L} \sim 140 \text{ fb}^{-1}$ and $\mathcal{L} \sim 36 \text{ fb}^{-1}$ integrated luminosities, respectively.

¹The explicit expression can be found in Ref. [4].

Results for the total and differential cross sections are in good agreement with the corresponding SM predictions [31–34].

The expressions provided in section 2 for the diboson cross section are obtained at the leading order (LO) in QCD. Higher order corrections can be included via the multiplicative K -factor relating the LO and NNLO cross section that, for $\sqrt{S} = 13$ TeV, is $K \simeq 1.721$ [34]. We assume that the K factors enhance the anomalous terms in the same way as the SM contribution. The mild dependence of the NNLO corrections on m_{WW} [31, 32, 34] can be safely neglected on the considered range of the diboson invariant masses.

3.1 LHC: run2 and high-luminosity phase

Following the ATLAS analyses in Refs. [29, 30, 39], we consider six bins Δ_i for the diboson invariant mass, with edges given by

$$\Delta_i = \left\{ [2M_W/\text{GeV}, 200], [200, 300], [300, 450], [450, 600], [600, 1200], [> 1200] \right\}, \quad (3.1)$$

see Fig.14h in [39] (where $m_{T,e\mu}$ coincides with our m_{WW} in the W^+W^- CM frame). To constrain the unitarity violation parameters δ_q we then utilize a χ^2 test set at the 95% confidence level (CL)

$$\chi^2(\delta_q) = \sum_{i=1}^6 \frac{\left(\alpha_i \bar{\sigma}_i(\delta_q) - r_i \right)^2}{\varepsilon_i^2} \leq 12.592, \quad (3.2)$$

where the index i runs over the specified bins Δ_i with experimental error ε_i and central values r_i for the ratio of data/SM yield. The cross sections $\bar{\sigma}_i(\delta_q)$ are obtained by integrating Eq. (2.1) over the solid angle and in each bin:

$$\bar{\sigma}_i(\delta) \equiv \int_{\Delta_i} \frac{d\sigma(\delta)}{dm_{WW} d\Omega} dm_{WW} d\Omega. \quad (3.3)$$

The value obtained for $\delta_q = 0$ recovers the corresponding SM cross section $\bar{\sigma}_i^{\text{SM}} \equiv \bar{\sigma}_i(0)$, which we utilize to compute the factors $\alpha_i \equiv r_i/\bar{\sigma}_{\text{SM}}$ that correct for the normalization used in the experimental data, the collider luminosity as well as for the branching ratio and selection efficiencies involved in the search.

We assume that the parameters δ_q are independent quantities and perform χ^2 tests by retaining only one non-vanishing contribution at a time. The results obtained are reported in Fig. 2, in which we plot the χ^2 value as a function of the considered δ_q parameter for the cases of $q = u, c, d, s$. The projections for the high-luminosity phase of the LHC (HL-LHC) are obtained upon a rescaling of the experimental errors by a factor of $\sqrt{\mathcal{L}_{\text{LHC}}/\mathcal{L}_{\text{HL}}}$, where we take $\mathcal{L}_{\text{LHC}} = 140 \text{ fb}^{-1}$ and $\mathcal{L}_{\text{HL}} = 3000 \text{ fb}^{-1}$. The bounds for all δ_q parameters obtained at 95% CL are summarized in Tab. 1.

The up- and down-quark dominance in the proton PDF results in a larger sensitivity to the δ_u and δ_d parameters constrained below 2–4%, with the run2 data, and up to 0.3–0.6% with the increased luminosity of HL-LHC. Milder bounds are obtained for δ_s and δ_c , of order 10% and 20% with the run2 data and up to 2% and 5% at the HL-LHC, respectively. As for δ_b , looser constraints of about 30% and 10% are obtained in the two cases. The bounds in Tab. 1 are consistent with the results in Eqs. (1.3)–(1.6) due to flavor physics, which still provides the strongest bounds on the $\delta_{u,d,s,c}$ parameters. We stress that the bounds in Eqs. (1.3)–(1.6) are obtained through individual measurements of the involved V_{CKM} matrix elements. Conversely, the method suggested here directly probes the sum encapsulated in δ_q and, therefore, provides an independent complementary test that could be used along with the flavor physics results.

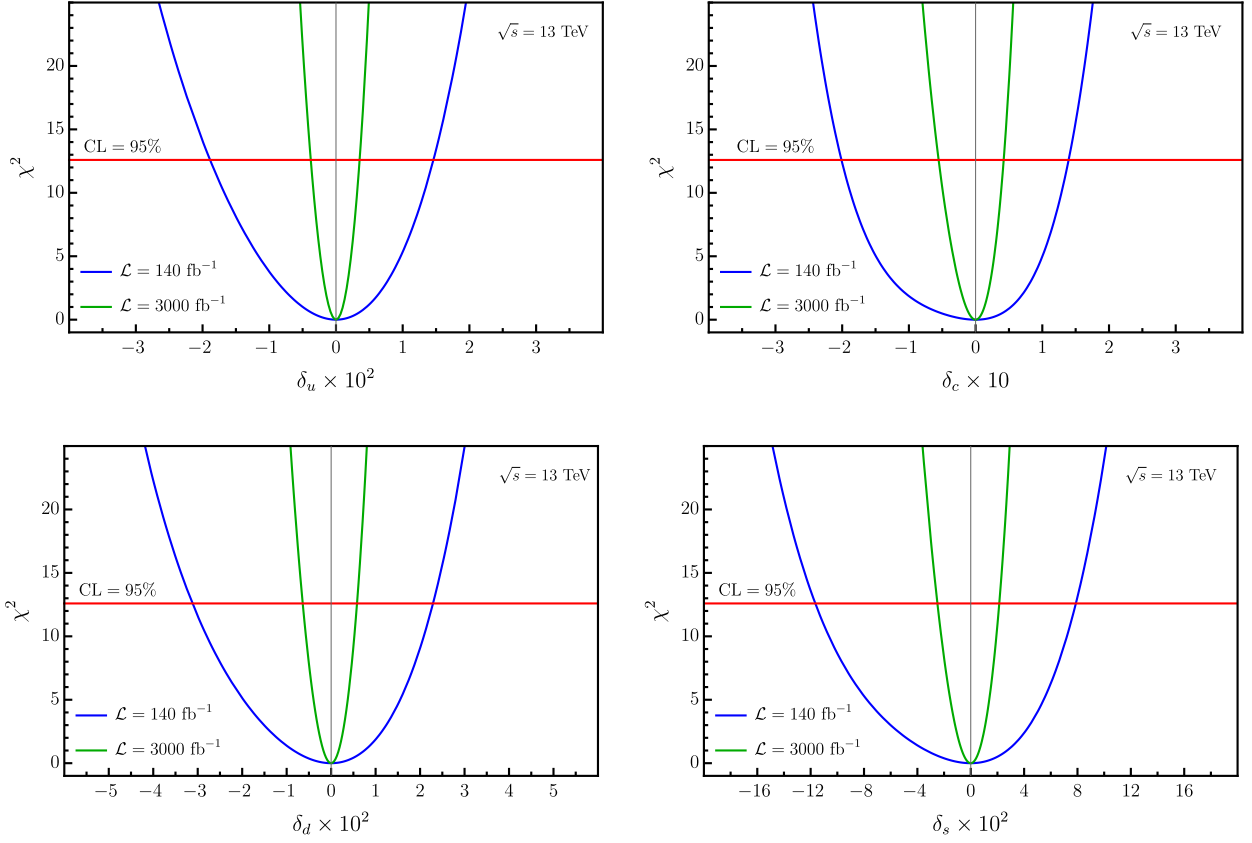


Figure 2: The χ^2 as a function of δ_u (first panel), δ_c (second panel), δ_d (third panel) and δ_s (fourth panel). The blue curve uses the run2 LHC data with integrated luminosity $\mathcal{L} = 140 \text{ fb}^{-1}$, while the green curve shows the corresponding HL-LHC reach for an integrated luminosity $\mathcal{L} = 3000 \text{ fb}^{-1}$. Values of the parameters yielding a χ^2 value above the red horizontal line are excluded at 95% CL.

95% CL	(run2) $\mathcal{L} = 140 \text{ fb}^{-1}$	(Hi-Lumi) $\mathcal{L} = 3000 \text{ fb}^{-1}$
δ_u	$-1.9 \times 10^{-2} < \delta_u < 1.5 \times 10^{-2}$	$-3.8 \times 10^{-3} < \delta_u < 3.5 \times 10^{-3}$
δ_d	$-3.1 \times 10^{-2} < \delta_d < 2.3 \times 10^{-2}$	$-6.4 \times 10^{-3} < \delta_d < 5.8 \times 10^{-3}$
δ_s	$-1.2 \times 10^{-1} < \delta_s < 7.9 \times 10^{-2}$	$-2.5 \times 10^{-2} < \delta_s < 2.1 \times 10^{-2}$
δ_c	$-2.0 \times 10^{-1} < \delta_c < 1.4 \times 10^{-1}$	$-5.5 \times 10^{-2} < \delta_c < 4.2 \times 10^{-2}$
δ_b	$-3.5 \times 10^{-1} < \delta_b < 2.6 \times 10^{-1}$	$-1.4 \times 10^{-1} < \delta_b < 8.8 \times 10^{-2}$

Table 1: Limits at 95% CL on the diagonal parameters δ_q obtained with LHC run2 data and corresponding HL-LHC projections.

3.2 Future circular collider

We extend the analysis to gauge the reach of the proposed method at the future circular hadron collider FCC-hh [35, 36], operating at $\sqrt{S} = 100$ TeV. For the computation of the cross section in Eq. (2.1) we use again the PDF4LHC21 PDFs given in Ref. [37] with $\sqrt{S} = 100$ TeV and factorization scale m_{WW} .

The distribution in m_{WW} , obtained by integrating the cross section on the full solid angle, is discretized over 9 benchmark bins defined by

$$\Delta_i^{\text{FCC}} = \left\{ [2M_W/\text{GeV}, 500], [500, 1000], [1000, 1500], [1500, 2000], [2000, 3000], [3000, 4000], [4000, 5000], [5000, 6000], [> 6000] \right\}, \quad (3.4)$$

in units of GeV. In order to constrain the δ_q parameters we then introduce the following χ^2 test

$$\chi^2(\delta_q) = \sum_{i=1}^9 \frac{(N_i(\delta_q) - N_i^{\text{SM}})^2}{N_i^{\text{SM}}} \leq 16.919 \quad (95\% \text{ CL}), \quad (3.5)$$

where $N_i(\delta_q)$ and $N_i^{\text{SM}} = N_i(0)$ are the expected number of events in the Δ_i^{FCC} bin in the presence of unitarity violation and in the SM, respectively. We set the related uncertainties to $\sqrt{N_i^{\text{SM}}}$ assuming that the experimental error will be dominated by the statistical one and include the NNLO QCD corrections accounting for a K -factor of $K \sim 1.58$, at $\sqrt{S} = 100$ TeV [33], in the computation of the number of events. For the integrated luminosity we consider the benchmark scenarios of $\mathcal{L} = 30 \text{ ab}^{-1}$ [36].

95% CL	(FCC-hh) $\mathcal{L} = 30 \text{ ab}^{-1}$
δ_u	$-9.5 \times 10^{-5} < \delta_u < 9.2 \times 10^{-5}$
δ_d	$-1.3 \times 10^{-4} < \delta_d < 1.3 \times 10^{-4}$
δ_s	$-2.4 \times 10^{-4} < \delta_s < 2.4 \times 10^{-4}$
δ_c	$-3.9 \times 10^{-4} < \delta_c < 3.9 \times 10^{-4}$
δ_b	$-7.4 \times 10^{-4} < \delta_b < 7.3 \times 10^{-4}$

Table 2: Forecasts for the 95% CL bounds obtained for the parameters δ_q , $q = u, d, s, c, b$ at the FCC-hh collider with $\sqrt{S} = 100$ TeV and integrated luminosity of 30 ab^{-1} .

In Tab. 2 we report the bounds obtained at 95% CL for the δ_q parameters. As we can see, the W^+W^- production at 100 TeV can potentially test the unitarity of the CKM matrix at a level of precision well on par with the present sensitivities obtained in flavor physics experiments Eqs. (1.3)–(1.4). In particular, the test restricts the $\delta_{u,d}$ and δ_s parameters below $\sim 1 \times 10^{-4}$ and $\sim 3 \times 10^{-4}$, respectively, while the magnitude of δ_c and δ_b can be probed to corresponding precisions of $\sim 4 \times 10^{-4}$ and $\sim 7 \times 10^{-4}$. Clearly, the inclusion of the background, detector effects and potential systematic effects would deteriorate the constraints show in Tab. 2, to an extent that can only be quantified after the machine will be well-understood.

4 Summary

We explore the potential of the W^+W^- production cross section at hadron colliders to test violations of unitarity in the quark mixing, parameterized by the CKM matrix. By using the most recent ATLAS measurements of the observable, the proposed test constrains the diagonal unitarity violation parameters defined in Eq. (2.8) to a level of $|\delta_{u,d}| \lesssim \mathcal{O}(10^{-2})$ and $|\delta_{c,s}| \lesssim \mathcal{O}(10^{-1})$ for first and second quark generation, respectively. The amount of unitarity violation admitted by the LHC run2 data in the b sector is instead $|\delta_b| \lesssim 30\%$. We estimate that the bounds could improve roughly by a factor of order ~ 4 – 5 and ~ 3 – 4 for $\delta_{u,d,s}$ and $\delta_{c,b}$, respectively, with the planned high-luminosity LHC phase. We repeat the analysis to gauge the potential of the future FCC-hh hadron collider, operating at $\sqrt{S} = 100$ TeV and with a benchmark total integrated luminosity of 30 ab^{-1} . Due to the fact that the sensitivity of the $pp \rightarrow W^+W^-$ cross section to the δ_q parameters grows quadratically with the W^+W^- invariant mass, the constraints posed by the proposed unitarity test largely improve. Depending on the experimental sensitivity that will be achieved for the W^+W^- cross section in the range of high W^+W^- invariant mass, $m_{WW} \gtrsim 1$ TeV, the method can produce limits of order $|\delta_q| \lesssim \mathcal{O}(10^{-4})$ comparable, or even stronger, than the present bounds from flavor physics. The investigation can be straightforwardly extended to test also off-diagonal contributions to unitarity violations, corresponding to products of different rows, or columns, of the CKM matrix. Although it is currently difficult to assess the full potential of the proposed method, our work shows that it can provide independent strong bounds apt to complement the results of more traditional tests of unitarity violation.

Acknowledgements

The authors thank M. Fabbrichesi, M. Grazzini, T. Lagouri, R. Mazini and H. Veermäe for useful discussions. E.G. acknowledges the Department of Theoretical Physics of CERN for the kind hospitality during the preparation of this work. This work was supported by the Estonian Research Council grants PRG803, RVTT3 and by the CoE program grant TK202 “Fundamental Universe”.

Appendix A Analytical expressions

We provide below the complete analytical expressions for the quantities $\Delta\overline{\mathcal{M}}_{1,2}^{q\bar{q}}$ appearing in Eq. (2.9). For the up-type quarks, $U = u, c$, we have

$$\begin{aligned} \Delta\overline{\mathcal{M}}_1^{U\bar{U}} &= \frac{4\alpha^2\pi^2}{3N_c(1-\beta_W^2)^2(1+2\beta_W c_\Theta + \beta_W^2)^2(M_Z^2 - s)s_W^4} \left\{ 3s(1-\beta_W^2) \left[-8 - 24\beta_W c_\Theta \right. \right. \\ &- \beta_W^2(7+9c_\Theta^2) + 16\beta_W^3 c_\Theta + 2\beta_W^4(7+3c_\Theta^2+2c_\Theta^4) + 8\beta_W^5 c_\Theta^3 - 3\beta_W^6(1-c_\Theta^2) \left. \right] \\ &+ 2M_Z^2 \left[12 + 16\beta_W c_\Theta(3-s_W^2) + \beta_W^2(27+c_\Theta^2(33-26s_W^2) - 38s_W^2) \right. \\ &+ 4\beta_W^3 c_\Theta(3-24s_W^2 - c_\Theta^2(3-4s_W^2)) - 2\beta_W^4(15+s_W^2+3c_\Theta^2(3+s_W^2) + c_\Theta^4(6-4s_W^2)) \\ &- 4\beta_W^5 c_\Theta(9+3c_\Theta^2-20s_W^2) + \beta_W^6(3+30s_W^2+8c_\Theta^4 s_W^2 - c_\Theta^2(15-26s_W^2)) \\ &\left. \left. + 16\beta_W^7 c_\Theta^3 s_W^2 - 6\beta_W^8(1-c_\Theta^2)s_W^2 \right] \right\}, \end{aligned} \quad (\text{A.1})$$

$$\begin{aligned} \Delta\overline{\mathcal{M}}_2^{U\bar{U}} &= \frac{4\alpha^2\pi^2}{N_c(1-\beta_W^2)^2(1+2\beta_W c_\Theta + \beta_W^2)^2 s_W^4} \left\{ 4 + 16\beta_W c_\Theta + \beta_W^2(9+11c_\Theta^2) + 4\beta_W^3 c_\Theta(1-c_\Theta^2) \right. \\ &\left. - 2\beta_W^4(5+3c_\Theta^2+2c_\Theta^4) - 4\beta_W^5 c_\Theta(3+c_\Theta^2) + \beta_W^6(1-5c_\Theta^2) \right\}. \end{aligned} \quad (\text{A.2})$$

The analytical forms of the $\Delta\overline{\mathcal{M}}_{1,2}^{D\bar{D}}$ terms involving down-type quarks, $D = d, s, b$, can be obtained from the ones above through the global substitution $c_\Theta \rightarrow -c_\Theta$ and by the replacement $s_W^2 \rightarrow \frac{1}{2}s_W^2$ in the terms appearing inside the curly brackets. Definitions for the symbols appearing in Eqs. (A.1)–(A.2) can be found in section 2.

References

- [1] N. Cabibbo, *Unitary Symmetry and Leptonic Decays*, *Phys. Rev. Lett.* **10** (1963) 531–533.
- [2] M. Kobayashi and T. Maskawa, *CP Violation in the Renormalizable Theory of Weak Interaction*, *Prog. Theor. Phys.* **49** (1973) 652–657.
- [3] J. Charles et al., *Current status of the Standard Model CKM fit and constraints on $\Delta F = 2$ New Physics*, *Phys. Rev. D* **91** (2015), no. 7 073007, [[arXiv:1501.05013](#)].
- [4] **Particle Data Group** Collaboration, R. L. Workman and Others, *Review of Particle Physics*, *PTEP* **2022** (2022) 083C01.
- [5] J. C. Hardy and I. S. Towner, *Superallowed $0^+ \rightarrow 0^+$ nuclear β decays: 2020 critical survey, with implications for V_{ud} and CKM unitarity*, *Phys. Rev. C* **102** (2020), no. 4 045501.

- [6] A. Crivellin, M. Kirk, T. Kitahara, and F. Mescia, *Global fit of modified quark couplings to EW gauge bosons and vector-like quarks in light of the Cabibbo angle anomaly*, *JHEP* **03** (2023) 234, [[arXiv:2212.06862](#)].
- [7] Y. Grossman, E. Passemar, and S. Schacht, *On the Statistical Treatment of the Cabibbo Angle Anomaly*, *JHEP* **07** (2020) 068, [[arXiv:1911.07821](#)].
- [8] A. Crivellin, *Explaining the Cabibbo Angle Anomaly*, 7, 2022. [arXiv:2207.02507](#).
- [9] M. Kirk, *Cabibbo anomaly versus electroweak precision tests: An exploration of extensions of the Standard Model*, *Phys. Rev. D* **103** (2021), no. 3 035004, [[arXiv:2008.03261](#)].
- [10] C. A. Manzari, *Explaining the Cabibbo Angle Anomaly*, *PoS EPS-HEP2021* (2022) 526, [[arXiv:2111.04519](#)].
- [11] T. Kitahara and K. Tobioka, *MeV sterile neutrino in light of the Cabibbo-angle anomaly*, *Phys. Rev. D* **108** (2023), no. 11 115034, [[arXiv:2308.13003](#)].
- [12] C.-Y. Seng, *Towards a discovery of BSM physics from the Cabibbo angle anomaly*, *Mod. Phys. Lett. A* **37** (2022), no. 02 2230002, [[arXiv:2112.10942](#)].
- [13] A. K. Alok, A. Dighe, S. Gangal, and J. Kumar, *Leptonic operators for the Cabibbo angle anomaly with SMEFT RG evolution*, *Phys. Rev. D* **108** (2023), no. 11 113005, [[arXiv:2108.05614](#)].
- [14] W.-F. Chang, *One colorful resolution to the neutrino mass generation, three lepton flavor universality anomalies, and the Cabibbo angle anomaly*, *JHEP* **09** (2021) 043, [[arXiv:2105.06917](#)].
- [15] A. Crivellin, C. A. Manzari, and M. Montull, *Correlating nonresonant di-electron searches at the LHC to the Cabibbo-angle anomaly and lepton flavor universality violation*, *Phys. Rev. D* **104** (2021), no. 11 115016, [[arXiv:2103.12003](#)].
- [16] B. Capdevila, A. Crivellin, C. A. Manzari, and M. Montull, *Explaining $b \rightarrow s\ell^+\ell^-$ and the Cabibbo angle anomaly with a vector triplet*, *Phys. Rev. D* **103** (2021), no. 1 015032, [[arXiv:2005.13542](#)].
- [17] A. M. Coutinho, A. Crivellin, and C. A. Manzari, *Global Fit to Modified Neutrino Couplings and the Cabibbo-Angle Anomaly*, *Phys. Rev. Lett.* **125** (2020), no. 7 071802, [[arXiv:1912.08823](#)].
- [18] **ATLAS** Collaboration, G. Aad et al., *Measurement of W^+W^- production in pp collisions at $\sqrt{s}=7$ TeV with the ATLAS detector and limits on anomalous WWZ and $WW\gamma$ couplings*, *Phys. Rev. D* **87** (2013), no. 11 112001, [[arXiv:1210.2979](#)]. [Erratum: *Phys.Rev.D* 88, 079906 (2013)].
- [19] **ATLAS** Collaboration, G. Aad et al., *Measurement of total and differential W^+W^- production cross sections in proton-proton collisions at $\sqrt{s} = 8$ TeV with the ATLAS detector and limits on anomalous triple-gauge-boson couplings*, *JHEP* **09** (2016) 029, [[arXiv:1603.01702](#)].
- [20] **CMS** Collaboration, V. Khachatryan et al., *Measurement of the W^+W^- cross section in pp collisions at $\sqrt{s} = 8$ TeV and limits on anomalous gauge couplings*, *Eur. Phys. J. C* **76** (2016), no. 7 401, [[arXiv:1507.03268](#)].

- [21] **CMS** Collaboration, S. Chatrchyan et al., *Measurement of the W^+W^- Cross Section in pp Collisions at $\sqrt{s} = 7$ TeV and Limits on Anomalous $WW\gamma$ and WWZ Couplings*, *Eur. Phys. J. C* **73** (2013), no. 10 2610, [[arXiv:1306.1126](#)].
- [22] C. Degrande, N. Greiner, W. Kilian, O. Mattelaer, H. Mebane, T. Stelzer, S. Willenbrock, and C. Zhang, *Effective Field Theory: A Modern Approach to Anomalous Couplings*, *Annals Phys.* **335** (2013) 21–32, [[arXiv:1205.4231](#)].
- [23] R. Franceschini, G. Panico, A. Pomarol, F. Riva, and A. Wulzer, *Electroweak Precision Tests in High-Energy Diboson Processes*, *JHEP* **02** (2018) 111, [[arXiv:1712.01310](#)].
- [24] **CMS** Collaboration, A. Tumasyan et al., *Measurements of the electroweak diboson production cross sections in proton-proton collisions at $\sqrt{s} = 5.02$ TeV using leptonic decays*, *Phys. Rev. Lett.* **127** (2021), no. 19 191801, [[arXiv:2107.01137](#)].
- [25] **CMS** Collaboration, S. Chatrchyan et al., *Measurement of W^+W^- and ZZ Production Cross Sections in pp Collisions at $\sqrt{s} = 8$ TeV*, *Phys. Lett. B* **721** (2013) 190–211, [[arXiv:1301.4698](#)].
- [26] **CMS** Collaboration, A. M. Sirunyan et al., *W^+W^- boson pair production in proton-proton collisions at $\sqrt{s} = 13$ TeV*, *Phys. Rev. D* **102** (2020), no. 9 092001, [[arXiv:2009.00119](#)].
- [27] **ATLAS** Collaboration, *Measurement of the W^+W^- production cross section in proton-proton collisions at $\sqrt{s} = 8$ TeV with the ATLAS detector*, **ATLAS-CONF-2014-033**.
- [28] **ATLAS** Collaboration, M. Aaboud et al., *Measurement of the W^+W^- production cross section in pp collisions at a centre-of-mass energy of $\sqrt{s} = 13$ TeV with the ATLAS experiment*, *Phys. Lett. B* **773** (2017) 354–374, [[arXiv:1702.04519](#)].
- [29] **ATLAS** Collaboration, M. Aaboud et al., *Measurement of fiducial and differential W^+W^- production cross-sections at $\sqrt{s} = 13$ TeV with the ATLAS detector*, *Eur. Phys. J. C* **79** (2019), no. 10 884, [[arXiv:1905.04242](#)].
- [30] **ATLAS** Collaboration, *Measurements of W^+W^- production cross sections in pp collisions at $\sqrt{s} = 13$ TeV with the ATLAS detector*, **ATLAS-CONF-2023-012**.
- [31] Gehrmann, T. and Grazzini, M. and Kallweit, S. and Maierhöfer, P. and von Manteuffel, A. and Pozzorini, S. and Rathlev, D. and Tancredi, L., *w^+w^- production at hadron colliders in next to next to leading order qcd*, *Phys. Rev. Lett.* **113** (2014), no. 21 212001, [[arXiv:1408.5243](#)].
- [32] Grazzini, M. and Kallweit, S. and Pozzorini, S. and Rathlev, D. and Wiesemann, M., *w^+w^- production at the lhc: fiducial cross sections and distributions in nnlo qcd*, *JHEP* **08** (2016) 140, [[arXiv:1605.02716](#)].
- [33] D. de Florian, M. Grazzini, C. Hanga, S. Kallweit, J. M. Lindert, P. Maierhöfer, J. Mazzitelli, and D. Rathlev, *Differential Higgs Boson Pair Production at Next-to-Next-to-Leading Order in QCD*, *JHEP* **09** (2016) 151, [[arXiv:1606.09519](#)].
- [34] M. Grazzini, S. Kallweit, J. M. Lindert, S. Pozzorini, and M. Wiesemann, *NNLO QCD + NLO EW with Matrix+OpenLoops: precise predictions for vector-boson pair production*, *JHEP* **02** (2020) 087, [[arXiv:1912.00068](#)].
- [35] *Physics at the FCC-hh, a 100 TeV pp collider*, [arXiv:1710.06353](#).

- [36] **FCC** Collaboration, A. Abada et al., *FCC Physics Opportunities: Future Circular Collider Conceptual Design Report Volume 1*, *Eur. Phys. J. C* **79** (2019), no. 6 474.
- [37] **PDF4LHC Working Group** Collaboration, R. D. Ball et al., *The PDF4LHC21 combination of global PDF fits for the LHC Run III*, *J. Phys. G* **49** (2022), no. 8 080501, [[arXiv:2203.05506](https://arxiv.org/abs/2203.05506)].
- [38] **CMS** Collaboration, *Measurement of W^+W^- inclusive and differential cross sections in pp collisions at $\sqrt{s}=13.6$ TeV with the CMS detector*, .
- [39] **ATLAS** Collaboration, *Measurements of w^+w^- production cross sections in pp collisions at $\sqrt{s} = 13$ tev with the atlas detector*, 2023. [Webpage](#).